AN-92-16-4

COMPUTATIONAL SIMULATION OF KITCHEN AIRFLOWS WITH COMMERCIAL HOODS

R.M. Kelso, P.E. *Member ASHRAE*
L.E. Wilkening *Member ASHRAE*
E.G. Schaub
A.J. Baker, Ph.D., P.E.

ABSTRACT

An understanding of the details of air motion around and into supply/exhaust devices is important in the design and application of kitchen hoods. However, measurement and visualization of such air movement in laboratory environments are difficult and expensive. Theoretical analysis of complex turbulent mixed flows is not possible at this time, but a promising technique for study of air movement details involves numerical simulation that is termed computational fluid dynamics (CFD).

This paper presents results of CFD simulations of two-dimensional (planar) air motion in the vicinity of cooking surfaces, as modified by the presence of kitchen hoods of various designs. The CFD simulation codes are of new finite-element design, developed with partial support from ASHRAE research project RP-464.

Benchmark tests were conducted to determine suitable locations for farfield boundary conditions, with and without a thermal plume present. Two commercial hood designs were then modeled, with suitable meshings created to account for their geometrical and flow-bifurcation complexity. CFD simulations were conducted for a range of effective Reynolds numbers and for several Archimedes numbers. These results are compared and discussed in this paper.

INTRODUCTION

Statement of the Problem

Details of the capture of airborne contaminants by hoods that ventilate cooking equipment have been of interest to system designers for more than 50 years. However, the motion of airstreams in this environment is subtle and difficult to visualize or accurately measure, so efforts at flow field mapping have met with only limited success. It is believed by many researchers that the bulk of contaminants produced in cooking are released into the rising plume of heated air that originates at the heated surface and surrounds the cooking container. If this hypothesis is correct, the capture performance of hoods is directly related to the flow rate and flow path of the plume and to the motion and entrainment of air in the surrounding kitchen area.

Previous Work

In the 1950s, Thomas (1950) published hood inlet flow field maps derived from potential flow studies and laboratory experiments. By this time, the concept of "capture velocity," wherein the hood inlet potential flow-field velocities were assumed to be the means of capturing contaminants ejected from the cooking process with some opposing escape velocity, was widely accepted. Shortly thereafter, Hemeon (1963) published empirical equations for the flow rate of heated plumes and for the design of receiving hoods located over hot processes.

Fire codes (NFPA 1976) and mechanical codes (BOCA 1981) were originally based on the capture velocity concept. A companion paper elaborates on the history of code development for this subject. More recently, these codes have relied on fire performance testing at Underwriters' Laboratories and on manufacturers' tests. Neitzel (1982) lists empirical exhaust flow rates based on the type of equipment to be ventilated and, indirectly, to the heat released by the cooking. These studies have been supported by other investigators (Kelso 1981).

Other work has resulted in reporting of contaminant removal effectiveness of residential hoods under various conditions (Farnsworth et al. 1989). However, laboratory studies of plume and contaminant flow rates have been limited by available methods of measurement (Talbert et al. 1973), and designers and code officials have generally lacked definitive information.

The field of computational simulation of fluid dynamics systems offers potential as a tool for the study of contaminant distribution and air motion for the kitchen-hood environment. Computational fluid dynamics (CFD) methods constitute numerical techniques to approximately solve the equations of momentum, continuity, and energy at discrete locations (nodes) of a mesh covering the flow domain. The CFD results produce estimates of velocity, temperature, and contaminant concentration at each node, hence their spatial and temporal distributions, which can then be plotted to produce a visual record of the vector and scalar fields.

CFD research originated in the defense and aerospace industries and was first applied to the prediction of indoor air motion about 1974 (Nielsen 1974). Investigators in

Richard M. Kelso is a professor of architecture, **Lief E. Wilkening** and **Edward G. Schaub** are graduate students, and **A.J. Baker** is a professor of engineering science and mechanics at the University of Tennessee, Knoxville.

Japan (Murakami et al. 1988), Europe (Chen et al. 1990), and the U.S. (Baker and Kelso 1990) have been actively studying research issues and application of CFD methods to indoor flow-field prediction. CFD has the potential to be very useful in studying the relatively low-velocity air motion associated with the cooking process and to provide insight into the effects of airflow rates, heat inputs, external air currents, and methods of make-up air supply.

For a complete study, laboratory verification of CFD results is required. At this time, such laboratory data are not available and will not be for two years or so. In the meantime, the results of CFD computational sensitivity experiments, without laboratory verification, are valid for estimation purposes and also serve as an illustration of the technique. Further, these results should be in qualitative agreement with available empirical information and with expected fluid flow paths.

THE CFD PROCEDURE

Computational fluid dynamics (CFD) is the emerging science of fluid-thermal flow field simulation via generation of approximate solutions to the governing Navier-Stokes nonlinear partial differential equation (PDE) system. This PDE system is generally considered universally valid; however, many approximations must be made to yield a computationally tractible statement. First, since kitchen-hood flow fields are nonisothermal and typically weakly turbulent, an approximate constitutive closure model must be devised for the phenomenological description. Second, CFD numerical algorithms can only produce an approximate solution to these modeled equations. Thereby, numerical error mechanisms can and will compromise simulation accuracy, especially when computational meshes with inadequate resolution capabilities are used. This section briefly presents the key pertinent issues of the utilized CFD procedures.

The Problem Statement

A statistical manipulation of the Navier-Stokes PDE system is required to yield a computable form. The resultant construction is termed the "Reynolds-averaged Navier-Stokes (RINS)" equations, governing unsteady, incompressible flows. Following a suitable nondimensionalization, the simplest "turbulent viscosity" form of RINS in vector notation is

$$\mathfrak{L}(\rho_0) = \nabla \cdot u = 0, \tag{1}$$

$$\mathfrak{L}(u) = \frac{\partial u}{\partial t} + (u \cdot \nabla)u - \nabla \cdot \left(\frac{1}{\mathrm{Re}} + \nu^t\right)\nabla u + \nabla P - \mathrm{Ar}\,\Theta g = 0, \tag{2}$$

$$\mathfrak{L}(\Theta) = \frac{\partial \Theta}{\partial t} + (u \cdot \nabla)\Theta - \nabla \cdot \left(\frac{1}{\mathrm{RePr}} + \frac{\nu^t}{\mathrm{Pr}^t}\right)\nabla \Theta - s_\Theta = 0, \tag{3}$$

$$\mathfrak{L}(Y_A) = \frac{\partial Y_A}{\partial t} + (u \cdot \nabla) Y_A - \nabla \cdot \left(\frac{1}{\mathrm{ReSc}} + \frac{\nu^t}{\mathrm{Sc}^t}\right)\nabla Y_A - s_A = 0. \tag{4}$$

The dimensionless groups in Equations 2 through 4 are based on the definitions

$$\mathrm{Re} = \frac{UL}{\nu},$$

$$\mathrm{Gr} = \frac{g\,\beta\,(T_{max} - T_{min})\,L^3}{\nu^2},$$

$$\mathrm{Pr} = \frac{c_p \rho_0 \nu}{k},$$

$$\mathrm{Sc} = \frac{\nu}{D_{AB}} \tag{5}$$

where Re is the Reynolds number, Gr is the Grashof number, $\mathrm{Ar} \equiv \mathrm{GrRe}^{-2}$ is the Archimedes number, Pr is the Prandtl number, and Sc is the Schmidt number. A superscript t on any variable denotes its modeled "turbulent" counterpart.

The dependent variable set in Equations 1 through 4 includes mean velocity vector $u(x,t)$ with scalar resolution u_i, $1 \le i \le n$ for an n-dimensional problem, kinematic pressure ($P = p/\rho_0$), and potential temperature, $\Theta \equiv (T - T_{min})/(T_{max} - T_{min})$. In Equation 4, Y_A is the mass fraction of an inert species A, for example, a smoke tracer, and D_{AB} is the binary diffusion coefficient. Finally, the Boussinesq buoyancy body force approximation is made in Equation 2, and g is the gravity unit vector.

The solutions to Equations 1 through 4 are characterized by these nondimensional groups and by applied boundary conditions. Since second-order spatial derivatives are present in Equations 2 through 4, each isolated equation is elliptic for finite Reynolds number Re. Therefore, knowledge of the mean flow variables, their normal derivatives, and/or linear combinations thereof is required everywhere on the boundary $\partial\Omega$ of the spatial domain of definition $\Omega \subset \Re^n$. However, handling of the continuity equation (1) dominates the mathematical well-posedness issue of *any* proposed CFD theory.

Specifically, Equation 1 defines a differential constraint on velocity fields $u(x, t)$ that are admissible as solutions to Equations 2 and 3. This requirement intimately connects to the pressure (gradient) field acting as

a source in Equation 2. For incompressible or constant-density fluids, neither an algebraic equation (of state) nor a differential equation is available for determination of pressure. Pressure may be mathematically eliminated only via a dependent variable transformation to vorticity and stream function vector fields. Alternatively, several inexact CFD theories may be devised such that pressure effects are adequately simulated during a convergent iterative solution process. Three mathematically distinct forms have been derived, as summarized and documented in Baker et al. (1989).

Since these reported kitchen flow field simulations are restricted to two dimensions, the mathematically exact vorticity-stream function restatement of Equations 1 and 2 is selected. Hence, Equations 1 and 2 are replaced by Baker (1983, chapter 5):

$$\begin{aligned} \mathcal{L}(\omega) &= \frac{\partial \omega}{\partial t} + u \cdot \nabla \omega \\ &- \nabla \cdot \left(\frac{1}{\mathrm{Re}} + \nu^t \right) \nabla \omega - \mathrm{Ar} \nabla \\ &\times \Theta \hat{g} \cdot \hat{k} = 0, \end{aligned} \tag{6}$$

$$\mathcal{L}(\psi) = \nabla^2 \psi + \omega = 0 \tag{7}$$

where ω and ψ are the k components of the vorticity and stream function vectors. Their definitions are

$$u = \nabla \times \psi \hat{k}, \quad \omega = \nabla \times u \cdot \hat{k}. \tag{8}$$

Equations 3 and 4 are unchanged in this transformation.

Closure for Diffusion The RINS system, Equations 1 through 8, must be closed for turbulence effects via definition of a model for the distribution of kinematic eddy viscosity ν^t. A constitutive relationship, assumed between the Reynolds deviatoric stress tensor and the mean flow strain rate tensor, defines ν^t via Baker (1983, chapter 7):

$$-\left(\overline{u_i u_j} - \frac{2}{3} k \delta_{ij} \right) = \nu^t \left(\frac{\partial u_i}{\partial x_j} + \frac{\partial u_j}{\partial x_i} \right). \tag{9}$$

In Equation 9, k is the trace of the Reynolds stress tensor (called turbulent kinetic energy), and the similarity between Equation 9 and the Stokes laminar flow closure is quite evident. Several levels of single-point correlation models for ν^t have been devised, ranging from purely algebraic mixing-length (MLT) models to the turbulent kinetic energy-isotropic dissipation (TKE) two-equation system (Baker 1983, chapters 6, 7). Such models have an underlying assumption that the flow is fully turbulent and nominally unidirectional, and none works very satisfactorily outside its developmental range or for low-turbulence flows.

Since kitchen and kitchen-hood airflows are a very complex combination of low-turbulence and nonaerodynamic flows, a genuinely accurate turbulence closure model is unachievable at the present. However, for CFD comparative simulation purposes, the interplay between convective and diffusive mechanisms can be globally assessed via an effective diffusion parameter. The definition for turbulent Reynolds number (distribution) is

$$\mathrm{Re}^t = \frac{\nu^t}{\nu}. \tag{10}$$

Since one usually assumes that $\mathrm{Pr}^t \approx \mathrm{Pr}$ and $\mathrm{Sc}^t \approx \mathrm{Sc}$ in closing Equations 2 through 4, it is possible to extract common multipliers, yielding, for example, for Equation 2:

$$\left(\frac{1}{\mathrm{Re}} + \nu^t \right) \rightarrow \frac{1}{\mathrm{Re}} (1 + \mathrm{Re}^t). \tag{11}$$

As currently practiced, many CFD theories, hence code implementations, augment laminar (ν) and turbulent (ν^t) diffusion effects with "numerical diffusion" to achieve numerical stability. This can be interpreted as an "artificial" viscosity ν^a, and in the spirit of turbulent Reynolds number definition, one can define the artificial diffusion Reynolds number (distribution) $\mathrm{Re}^a \equiv \nu^a / \nu$.

Hence, in concert with Equation 11, this leads to the concept of an "effective" Reynolds number Re^f:

$$\mathrm{Re}^f = \frac{\mathrm{Re}}{1 + \mathrm{Re}^t + \mathrm{Re}^a}. \tag{12}$$

Clearly, from Equation 12, the least diffusive characterization corresponds to a laminar flow ($\mathrm{Re}^t \equiv 0$) simulation without added artificial viscosity. Thereafter, $\mathrm{Re}^t > 0$ and/or $\mathrm{Re}^a > 0$ serves basically (and mathematically) to increase diffusive effects and, hence, moderate sharp flow field features. For this basic CFD comparative characterization of kitchen-hood flow fields, we have elected to control Re^f to quantitatively compare the interplay between diffusive and convective flow mechanisms.

The CFD Model and Code

The reconstructed RINS system (Equations 6, 7, 3 through 5, and 11 and 12) is cast into a computable form via a finite-element (FE) procedure. The initial-boundary value equations (6, 3, and 4) for defining the effective diffusion coefficient $\nu^f \equiv (\mathrm{Re}^f)^{-1}$ are of the hyperbolic conservation law form,

$$\begin{aligned} \mathcal{L}(q) &= \frac{\partial q}{\partial t} + u \cdot \nabla q \\ &- \nabla \cdot (\nu_q^f \nabla q) - s_q = 0. \end{aligned} \tag{13}$$

The state variable for Equation 13 is the array $q(x,t) = \{\omega, \Theta, Y_A\}^T$, and s_q is the source term pertinent to each entry.

An FE construction for Equation 13 constitutes a semi-discretization of a weak statement written for Equation 13 for any approximation $q^N(x,t)$ to $q(x,t)$ (Baker and Pepper 1991). The resultant approximation error induced into Equation 13, i.e., $\mathcal{L}(q^N)$, is required to be

othogonal ("perpendicular") to the trial space supporting q^N via the Galerkin weak statement

$$WS^N = \int_\Omega \Psi_j(x)\, \mathcal{L}(q^N)\, d\tau = 0, \ \forall j \qquad (14)$$

for any approximation, i.e., $q(x,t) \ q^N(x,t) \equiv \Sigma \ \Psi_j(x) \ Q_j(t)$, $1 \leq j \leq N$. The FE formulation constructs a specific q^N using compact polynomial interpolations of each $\Psi_j(x)$ on the generic union of finite-element domains Ω_e sharing a node of the global disretization $\Omega^h \equiv \cup \Omega_e$ of the spatial domain of definition for Equation 13.

The resulting semi-discrete WS^N, denoted WS^h, always produces the matrix ordinary differential equation (ODE) system,

$$WS^h = [M] \frac{d\{Q\}}{dt} + \{R(Q)\} = \{0\}. \qquad (15)$$

In Equation 15, $[\bullet]$ and $\{\bullet\}$ denote a square and column matrix, respectively, and $\{Q\} \equiv \{Q(t)\}$ is the array of the state variable semi-discretization at the nodes of Ω^h. Any ODE algorithm utilizes Equation 15 to evaluate derivative terms in the Taylor series. The terminal "computable" algebraic statement is

$$\begin{aligned} \{FQ\} &= [M]\{Q_{n+1} - Q_n\} \\ &+ \Delta t(\theta\{R\}_{n+1} + (1-\theta)\{R\}_n) = \{0\} \end{aligned} \qquad (16)$$

upon selecting the θ-implicit, one-step (Euler/trapezoidal) ODE method, where $t_{n+1} = t_n + \Delta t$. The FE algorithm statement (Equation 16) is then completed with the WS^h for Equation 7, which yields

$$\{F\Psi\} = [D]\{\Psi\} + \{s\} = \{0\} \qquad (17)$$

where $[D]$ is the "diffusion" matrix equivalent of $(\nabla^2)^h$, the discretized Laplacian operator on Ω^h, and $\{s\}$ contains the source (vorticity) term from Equation 7.

Equations 16 and 17 constitute a nonlinear algebraic system for any $\theta > 0$. Associated matrix linear algebraic solution procedures amount to approximations to the generic Newton statement

$$[J]\{\delta Q\}^{p+1}_{n+1} = -\{F\}^p_{n+1} \qquad (18)$$

where the Jacobian definition is $[J] \equiv \partial\{F\}/\partial\{Q\} = [M] + \theta\Delta t\partial\{R\}/\partial\{Q\}$, and p is the iteration index at time t_{n+1}.

The available theory (Noronha 1989) characterizing the FE algorithm (Equations 14 through 18) confirms that a kth degree polynomial FE basis nominally produces a spatially $2k$ order-accurate algorithm, for bounded Re, on an adequate discretization Ω^h. For the trapezoidal rule, $\theta = 1/2$ in Equation 16, any WS^h basis implementation algorithm is free from artificial viscosity ν^a, hence $Re^a = 0$ in Equation 12.

DISCUSSION AND RESULTS

The CFD studies conducted are for flows existing on a vertical symmetry plane perpendicular to the long axis of a hood. This gives a region wherein the flow is approximately two dimensional (see Figure 1). For the level of velocity (i.e., Mach number) encountered in the problem class of interest, air behaves as an incompressible fluid. Normal cooking operations typically span several minutes, so that start-up and transient conditions are of minor importance in comparison to the steady state. Dissipative (laminar and/or "turbulent" diffusion) effects, which are important at cooking surfaces, back walls, and hood surfaces, as well as at plume and jet boundaries, are simulated via the effective Reynolds number model. For nonisothermal conditions, the importance of the buoyancy term in Equation 2 is characterized by the Archimedes number, $Ar = Gr/Re^2$. With low velocities and modest temperature differences, the Boussinesq approximation is thoroughly appropriate.

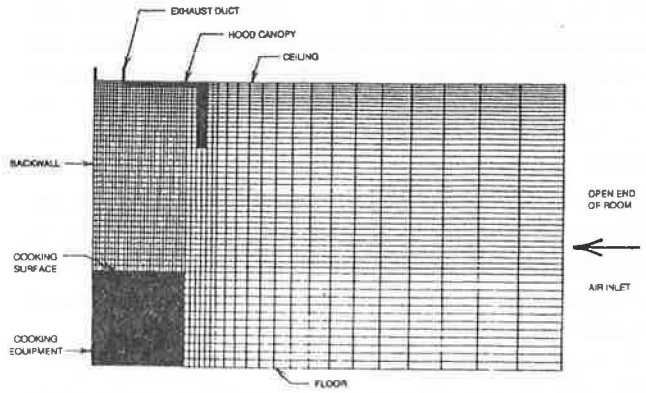

Figure 1 Vertical section through kitchen showing 50 × 50 computational mesh.

Thus, the flow class of this study is two dimensional, incompressible, thermal, and diffusive, and the steady-state solution is sought. The first model is a conventional exhaust hood with a uniform onset flow approaching from the opposite end of the room and exhausting up through the hood. A 50 × 50 nonuniform finite-element mesh (Figure 1) was used for modeling the flow field. Finer mesh spacings exist in wall regions in the area of the hood and the upper left corner of the exhaust outlet flow. For nominal onset flow of 0.6 ft/s, a 9-ft ceiling, and room temperature air, Re = 34,000 and Re^f would be approximately 1,000 (see Equation 12). The cooking surface temperature ranged to 300°F, hence for 70°F inlet air, $Gr \leq 3 \times 10^{11}$. The corresponding Archimedes number range is $0 \leq Ar \leq 285$.

Figure 2 plots the obtained steady-state velocity vector field for $Re^f = 100$ and isothermal conditions (Archimedes number Ar = 0). Flow enters from the right with uniform velocity. The plane of the hood canopy, to the left in the figure, is just forward of the leading edge of the cooking equipment. Flow exits the field vertically in the upper left corner within the hood. The inlet velocity of 0.6 fps, through the 9-foot-high opening, gives a flow rate of approximately 325 cfm per foot of hood length. This is a typical flow rate found in many hood instal-

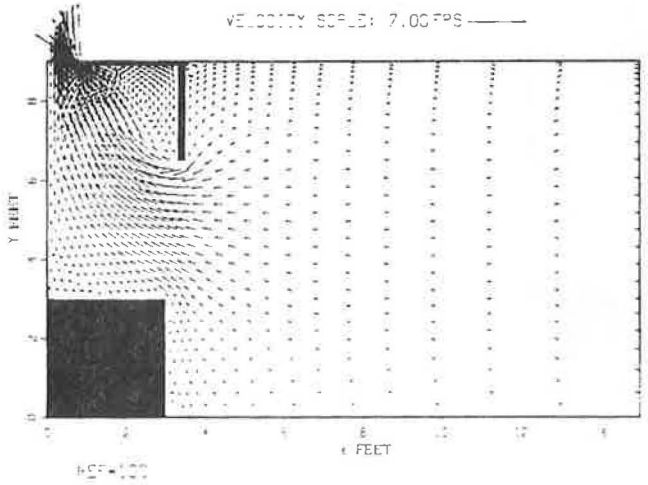

Figure 2 *Velocity vectors, isothermal conditions, conventional exhaust hood, 325 cfm/ft.*

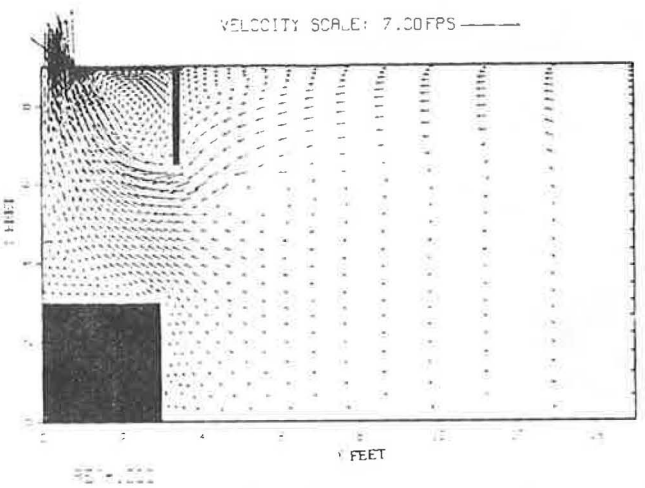

Figure 3 *Velocity vectors, isothermal conditions, conventional exhaust hood, 325 cfm/ft.*

lations. The flow accelerates rapidly into the opening between the hood and the leading edge of the cooking equipment, and recirculation regions are observed at the back corner of the cooking surface and inside the hood canopy. Such recirculation regions have been observed in the field (Hemeon 1963) and are predicted to occur in real flow.

Figures 2 through 4 show the flow fields as the Re^f is computationally increased from 100 to 2,000 as diffusive mechanisms become smaller. In all velocity vector plots except Figure 8, only every other vector in the Y-direction is plotted. Note the increasing size of recirculation regions, boundary layers becoming visible, and the formation of an eddy at human head height just in front of the hood. Because the grid is rather sparse in this area, this eddy may be a numerical aberration. Figure 3, with $Re^f = 1000$, approximates the low turbulence flow conditions found in many actual rooms.

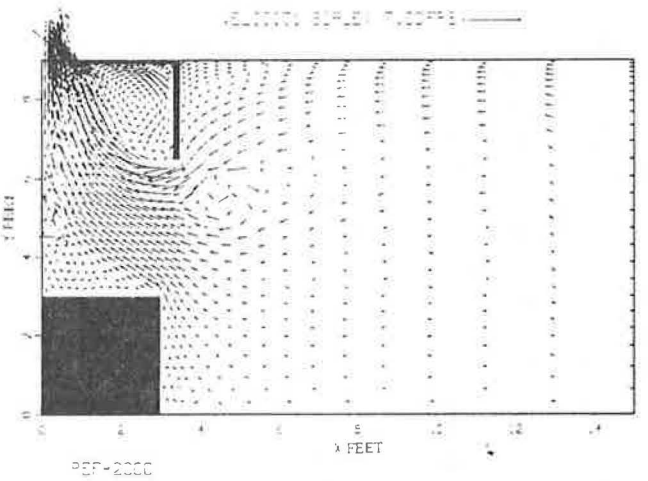

Figure 4 *Velocity vectors, isothermal conditions, conventional exhaust hood, 325 cfm/ft.*

An adequate mesh is an inescapable requirement of CFD modeling (Baker and Kelso 1990). Since the CFD process involves discretization of a continuum, any gridding of the flow field involves compromise and, as the elements become larger, the modeling becomes less accurate. Figure 5 is the CFD model of the same flow field, under the same conditions as Figure 2, but with a 40 × 30 mesh (1,200 grid points), as compared to the 50 × 50 mesh (2,500 grid points) used in the other figures. One of the symptoms of an inadequate mesh is "two delta x" oscillations, wherein values at adjacent grid points take on widely differing values. The "wild" oscillations in velocity at the corner of the cooking surface confirm this mesh is inadequate to resolve the flow field specification, even at $Re^f = 100$.

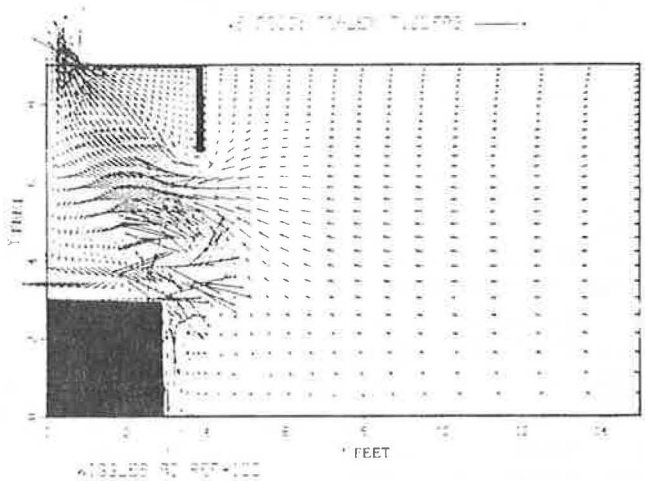

Figure 5 *Velocity vectors, isothermal conditions, 40 × 30 mesh, 325 cfm/ft.*

The addition of thermal effects has a large influence on the flow field. Figures 6 through 8 are velocity vector plots with thermal effects (energy equation included). Figure 7 has the same conditions as Figure 3, but with the inlet air temperature at 70°F and the cooking surface at

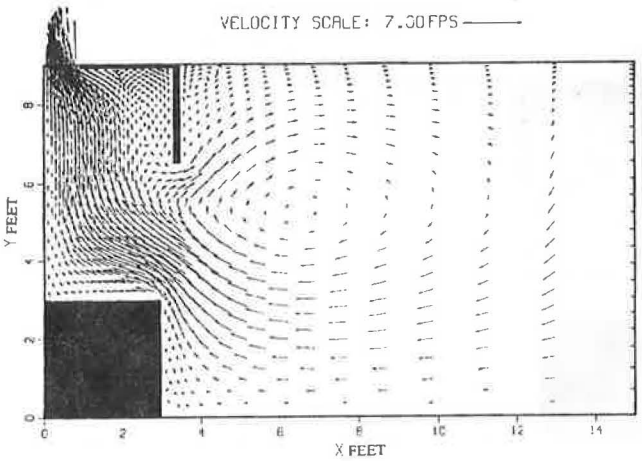

Figure 6 *Velocity vectors, thermal conditions, Ar = 285, 325 cfm/ft, cooking surface—300°F, air—70°F, Re^f = 2,000, temperature difference = 230.*

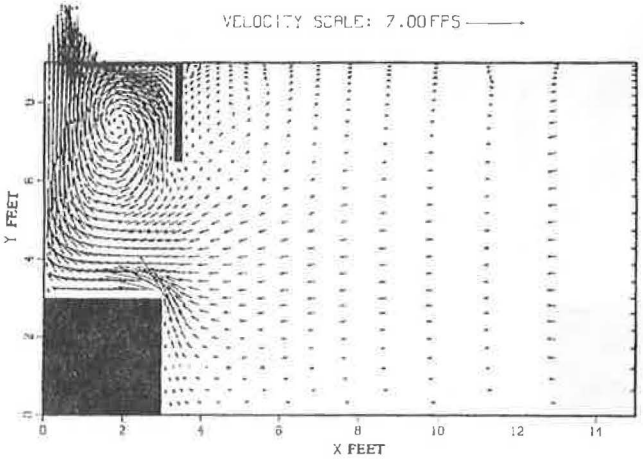

Figure 7 *Velocity vectors, thermal conditions, Ar = 285, 325 cfm/ft, cooking surface—300°F, air—70°F, Re^f = 4,000, temperature difference = 230.*

300°F (Ar = 285), simulating a griddle. Other surfaces are adiabatic (homogeneous Neumann conditions). Note the surface effect at the wall behind the griddle, where the heated plume increases the vertical flow rate and the recirculation region observed in Figures 2 through 7 disappears. Also of interest is the flow escaping from the hood under the front edge and the large eddy in front of the hood (Figure 6), similar to the isothermal case of Figures 3 and 4. Recirculation flow extends along the ceiling to the right almost to the inlet. Here also the grid spacing is too coarse to give confidence in the results. Figures 9 and 10 are plots of temperature contours at approximately 7°F intervals.

As the Re^f is increased to 1,000 in Figure 7, the surface effect increases and a well-defined recirculation region has developed in the hood. The flow that apparently escapes under the front edge of the hood has decreased and, outside the hood, the eddy at head height has disappeared and the ceiling recirculation has decreased. The temperature contours in Figure 10 are confined to the hood area. Note the wall area above the griddle, where temperature contours indicate increased plume flow rate and velocity. The heavy lines in Figures 9 and 10, where $x > 8$ indicates numerical 2 delta-x errors whose temperature differences are very small.

While the results of CFD modeling presented herein can hardly be considered quantitative, some qualitative observations can be made. Those involved with kitchen ventilation systems can confirm from field observations the surface effects of the wall behind the griddle and the escaping billows at the front edge of the hood when the exhaust flow rate is low. The important differences in flow fields when hot surfaces are introduced are well illustrated. It is hypothesized that the exhaust flow rate necessary to prevent escape of contaminated air is highly dependent on the rate of heat transfer by the cooking

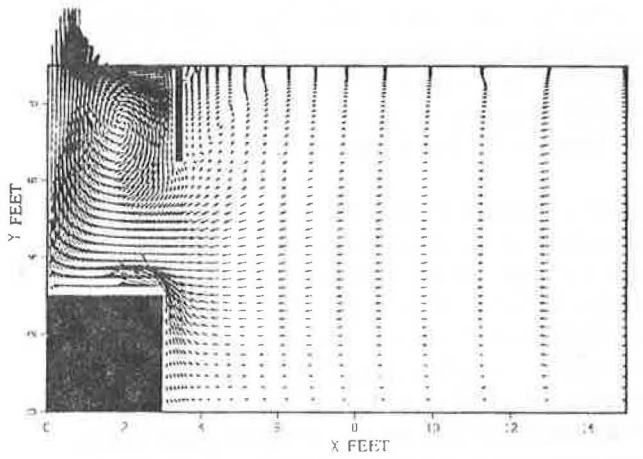

Figure 8 *Velocity vectors, thermal conditions, Ar = 285, all vectors plotted. Hood Re^f = 4,000, temperature difference = 230.*

process. This hypothesis is strengthened by comparing Figures 3 (isothermal) and 7 (thermal, Ar = 285).

An example of a hood that incorporates makeup air supply is the air curtain hood system depicted in Figure 11. In this hood, a stream of air is introduced vertically downward along the front edge of the hood. This air may be tempered or untempered. Typical flow rates are 30% of the exhaust flow rate supplied from the room and 70% from the air curtain. An inlet velocity of 3.3 fps is representative and is used in the isothermal flow field depicted in Figure 11 at Re^f = 1000. The 3.3-fps inlet velocity through a 10-in. opening gives an air curtain flow rate of 165 cfm/ft, and the 0.13 fps inlet velocity through the 9-ft-high room inlet gives a flow rate of 70 cfm/ft. Such bifurcated inlet conditions are particularly difficult for CFD models to solve.

Figure 11 is comparable to Figure 3 at Re^f = 1000 and isothermal conditions. The air curtain flow diverts the

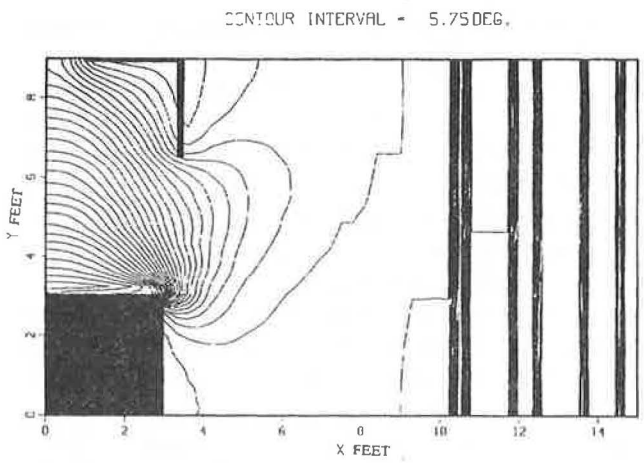

Figure 9 *Temperature contours, Ar = 285, conventional hood 325 cfm/ft, cooking surface—300°F, air—70°F, Re^f = 2,000, temperature difference = 230.*

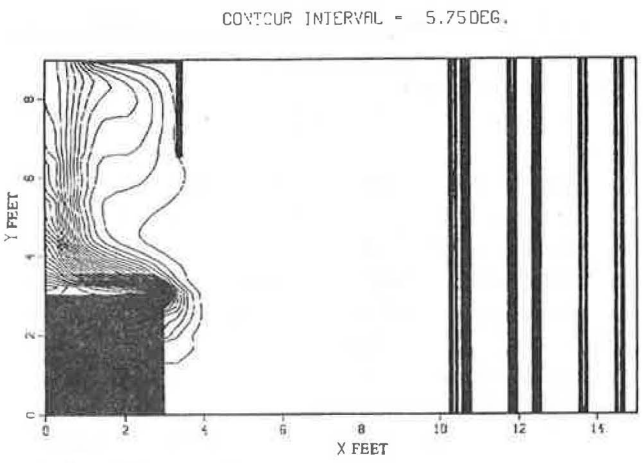

Figure 10 *Temperature contours, Ar = 285, conventional hood 325 cfm/ft, cooking surface—300°F, air—70°F, Re^f = 4,000, temperature difference = 230.*

flow from the room downward and directs it across the cooking surface, reducing the strength of the recirculation regions. High-velocity flow is confined to the upper region of the hood, and no evidence of escaping flow is seen.

Figure 12 is under conditions similar to Figure 11 but with thermal effects. The inlet airstreams are at 70°F and the griddle surface at 300°F. As was seen when comparing Figure 3 with Figure 7, the heated surface produces a plume that radically alters the flow field. Figure 12 shows that the excess plume flow rate turns down the inside of the canopy, enabling the air curtain to reach almost to the cooking surface. Flow pattern disturbances reach out into the room, well upstream of the hood.

CONCLUSIONS

The simulations shown conform qualitatively to field observations and expectations. They lend confidence to the concept of computational fluid dynamics (CFD) simulation of flow fields in rooms. They also reveal subtleties of the flow that may be useful to workers in the kitchen ventilation field.

Much work is ahead. The two-dimensional work shown here must be extended to three dimensions. The CFD models must be compared with laboratory tests and refined if necessary. Other conditions of flow rates, temperatures, and hood configurations must be simulated and tested. Means of modeling filters should be developed and their effects tested.

REFERENCES

Baker, A.J. 1983. *Finite element computational fluid mechanics*. Washington, DC: Hemisphere.

Baker, A.J., and R.M. Kelso. 1990. On validation of computational fluid dynamics: Procedures for room

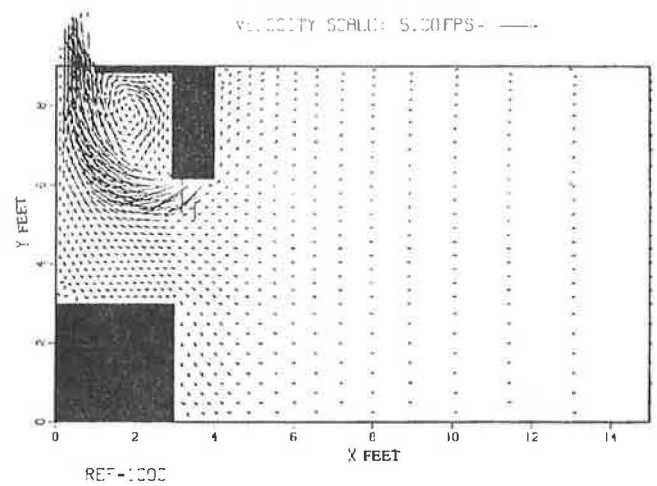

Figure 11 *Velocity vectors, isothermal conditions, Ar = 0, 325 cfm/ft, air curtain hood.*

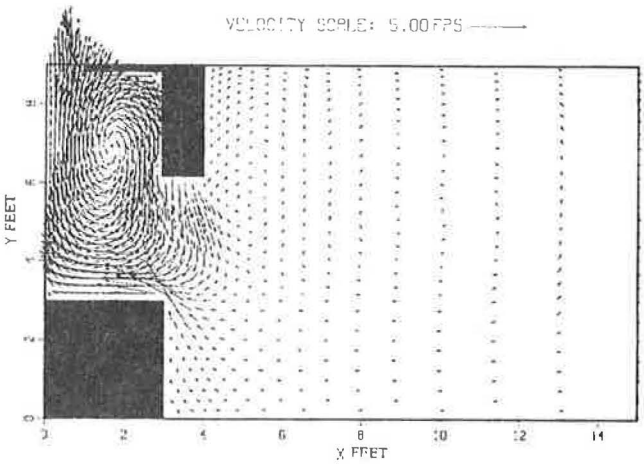

Figure 12 *Velocity vectors, thermal conditions, Ar = 285, 325 cfm/ft, max TD = 230°F, air curtain hood, Re^f = 4,000.*

air motion prediction. *ASHRAE Transactions* 96(1): 760-744.

Baker, A.J., and D.W. Pepper. 1991. *Finite elements 1-2-3*. New York: McGraw-Hill.

Baker, A.J., R.M. Kelso, W.P. Noronha, and J.B. Woods. 1989. On the maturing of computational fluid dynamics in design of room air ventilation systems. *Building Systems: Room Air and Air Contaminant Distribution*. Atlanta: American Society of Heating, Refrigerating, and Air-Conditioning Engineers, Inc.

BOCA. 1981. Basic building code, section M-3120, commercial hoods and fans. Building Owners and Code Officials.

Chen, Q., A. Moser, and A. Huber. 1990. Prediction of buoyant, turbulent flow by a low-Reynolds-number k-ε model. *ASHRAE Transactions* 96(1): 564-573.

Dalle Valle, J.M. 1953. Design of kitchen range hoods. *Heating and Ventilating* 50 (Aug.): 95.

Farnsworth, C., A. Waters, R.M. Kelso, and D. Fritsche. 1989. Development of a fully vented gas range. *ASHRAE Transactions* 95(1): 759-768.

Hemeon, W.C.L. 1963. *Plant and process ventilation*, 2d ed. New York: The Industrial Press.

Kelso, R.M. 1981. Kitchen range hoods and energy conservation. Proc. Int. Sym. on Indoor Air Pollution, Health and Energy Conservation, University of Massachusetts, Amherst.

Murakami, S., S. Kato, and Y. Surgama. 1988. Numerical and experimental study on turbulent diffusion fields in conventional flow type clean rooms. *ASHRAE Transactions* 94(2): 469-493.

Neitzel, E. 1982. Basic principles and relationships that exist in kitchen ventilation systems. Greenbeck Fan Co., unpublished research report.

NFPA. 1976. *NFPA 96, Standard for the installation of equipment for the removal of smoke and grease-laden vapors from commercial cooking equipment*. Boston: National Fire Protection Association.

Nielsen, P.V. 1974. Prediction of air flow and comfort in air conditioned spaces. *ASHRAE Transactions* 81(2).

Noronha, W. 1989. Accuracy and convergence of finite element incompressible Navier-Stokes algorithms. Ph.D. dissertation, University of Tennessee, Knoxville.

Talbert, S.G., L.J. Flanigan, and J.A. Eibling. 1973. An experimental study of ventilation requirements of commercial electric kitchens. *ASHRAE Transactions* 80.

Thomas, F.A., Jr. 1950. Design characteristics of canopy exhaust hoods. *Heating and Ventilating*, April.